



CHORUS

This is the accepted manuscript made available via CHORUS. The article has been published as:

Benefit from Photon Recycling at the Maximum-Power Point of State-of-the-Art Perovskite Solar Cells

Roberto Brenes, Madeleine Laitz, Joel Jean, Dane W. deQuilettes, and Vladimir Bulović

Phys. Rev. Applied **12**, 014017 — Published 10 July 2019

DOI: [10.1103/PhysRevApplied.12.014017](https://doi.org/10.1103/PhysRevApplied.12.014017)

Benefit from Photon Recycling at the Maximum Power Point of State-of-the-Art Perovskite Solar Cells

Roberto Brenes^{1,2, †}, Madeleine Laitz^{1,2, †}, Joel Jean^{1,3}, Dane W. deQuilettes², Vladimir Bulović^{1,2*}

¹Department of Electrical Engineering and Computer Science, Massachusetts Institute of Technology, 77 Massachusetts Avenue, Cambridge, Massachusetts 02139, USA

² Research Laboratory of Electronics, Massachusetts Institute of Technology, 77 Massachusetts Avenue, Cambridge, Massachusetts 02139, USA

³ Swift Solar Inc., Golden, Colorado 80401, USA

†Equal Contribution

*Corresponding Author: bulovic@mit.edu

Abstract

Photon recycling is required for a solar cell to achieve an open-circuit voltage (V_{oc}) and power conversion efficiency (PCE) approaching the Shockley-Queisser theoretical limit. The achievable performance gains from photon recycling in metal halide perovskite solar cells remain uncertain due to high variability in material quality and the non-radiative recombination rate. In this work, we quantify the enhancement due to photon recycling for state-of-the-art perovskite $\text{Cs}_{0.05}(\text{MA}_{0.17}\text{FA}_{0.83})_{0.95}\text{Pb}(\text{I}_{0.83}\text{Br}_{0.17})_3$ (triple-cation) films and corresponding solar cells. We show that, at the maximum power point (MPP), the absolute PCE can increase up to 2.0% in the radiative limit, primarily due to a 77 mV increase in (V_{MPP}). For this photoactive layer, even with finite non-radiative recombination, benefits from photon recycling can be achieved when non-radiative lifetimes and external LED electroluminescence efficiencies measured at open-circuit, $Q_e^{LED}(V_{oc})$, exceed 2 μs and 10%, respectively. This analysis quantifies the significance of photon recycling in boosting the real-world performance of perovskite solar cells toward theoretical limits.

I. Introduction

Improving solar cell power conversion efficiency (PCE) requires both optimization of device architectures and an understanding of fundamental photophysics. For example, PCEs of GaAs cells increased from 25.1% to 28.8% through photon management [1–4]. In luminescent optoelectronic materials, such as GaAs, photons can undergo multiple absorption and emission events before escaping, a phenomenon called photon recycling. During steady-state operation, photon recycling increases the charge carrier density within the photoactive cell layers, resulting in a higher quasi-Fermi level energy splitting (μ) and increased open-circuit voltage (V_{oc}) through $\mu = qV_{oc}$ [4–7]. Photon recycling also slows the external photon emission rate, decreasing the radiative saturation current [8,9]. Together, these effects can boost the performance of high-efficiency solar cells toward the Shockley-Queisser theoretical limit. To take advantage of photon recycling, a photovoltaic (PV) absorber material must exhibit a small Stokes shift, strong band-edge absorption, and high photoluminescence quantum efficiency (PLQE) [3–5,10–12].

Relatively low PLQEs have thus far limited the extent of photon recycling observed in perovskite thin films and single crystals [13–15]. Low PLQEs of <15% result from high first-order non-radiative recombination rates, (k_1) on the order of 10^6 to 10^9 s⁻¹, which are associated with trap state densities of 10^{15} to 10^{17} cm⁻³ [16–18]. For example, Pazos-Outón *et al.* demonstrated that the average photon only undergoes one recycling event in a typical CH₃NH₃PbI₃ film, but predicted that up to 25 recycling events could be sustained with a sufficiently high-quality sample [13]. This is in contrast to GaAs films used in state-of-the-art PV devices, where an average photon can participate in up to 50 recycling events [3]. In thick perovskite single crystals, several reports have used time-resolved photoluminescence spectroscopy to show a characteristic red-shift in emission spectra over time due to photon recycling [13]. This phenomenon is expected to be efficient in single crystals, which exhibit low bulk defect densities ($\sim 10^{10}$ cm⁻³). However, the high surface recombination velocities of 5,800 cm s⁻¹ lead to rapid quenching of excess carriers, diminishing the probability of photon recycling [14,19–23].

Passivated perovskite thin films with record-low non-radiative recombination rates and defect densities have achieved internal PLQEs exceeding 90% [18,24,25] — approaching the highest-quality double-heterostructured GaAs films [26]. These recent advances in material quality should enable improved photon recycling and light management in perovskite devices, but

thus far it has been unclear how to realize practical efficiency gains. Furthermore, other works have only considered the impact of photon recycling on perovskite solar cells at open-circuit, where the extent of recycling differs significantly from operation at the maximum power point (MPP). Under operation, rapid charge extraction reduces the steady-state carrier density, allowing non-radiative processes to compete with radiative recombination and photon recycling. The practical importance of photon recycling in perovskite solar cells thus remains unclear.

Here we perform a theoretical analysis of photon recycling in state-of-the-art $\text{Cs}_{0.05}(\text{MA}_{0.17}\text{FA}_{0.83})_{0.95}\text{Pb}(\text{I}_{0.83}\text{Br}_{0.17})_3$ (triple-cation) films, which, in photovoltaic devices, have demonstrated record efficiencies and high stability [27,28]. We examine the impact of photon recycling at the MPP with varying first-order non-radiative recombination rates and external emission efficiencies [29,30]. The analysis is extended to $\text{CH}_3\text{NH}_3\text{PbI}_3$ films, which have been extensively studied previously, serving as a benchmark to compare emerging perovskite formulations (see Supplemental Material Figs. S21-S28 [31]). Our model reveals the changes in carrier density and luminescence efficiency at MPP attributable to photon recycling and identifies optoelectronic material quality targets— i.e., external luminescence quantum efficiency and non-radiative recombination rates – toward which the community can strive. Quantifying these values is critical, as several reports have shown that devices with low non-radiative recombination can achieve V_{oc} deficits below 0.4 V, which is the deficit regime in which GaAs solar cells began to benefit from photon recycling [2,32–36].

II. Photon Recycling in the Detailed Balance Model

A. Radiative Limit

To quantify the effect of photon recycling on device performance, current-voltage (J-V) curves were simulated using a detailed balance model and experimentally determined absorption coefficient and refractive index data for $\text{Cs}_{0.05}(\text{MA}_{0.17}\text{FA}_{0.83})_{0.95}\text{Pb}(\text{I}_{0.83}\text{Br}_{0.17})_3$ (see Supplemental Material Fig. S8 [31]) [16,29]. In the Supplemental Material, we discuss key assumptions used in the model, which are consistent with previous analyses [7,13,29,31,37–39].

We first perform a detailed-balance calculation in the radiative limit (i.e., no non-radiative recombination, $k_1 = 0$) by equating the generation current with the recombination and extraction currents. The total current (J_{total}) as a function of voltage (V) is then defined as:

$$(1) \quad J_{total}(V) = J_{SC} - J_0^{rad,ext}(V)$$

where J_{SC} is the short-circuit current density

$$(2) \quad J_{SC} = q \int_0^\infty a(E) \phi_{sun}(E) dE$$

and $J_0^{rad,ext}$ is the external radiative saturation current, defined as the photon flux that escapes the film into the surrounding atmosphere multiplied by the fundamental charge, q :

$$(3) \quad J_0^{rad,ext}(V) = q\pi e^{\frac{qV}{kT}} \int_0^\infty a(E) \phi_{bb}(E) dE$$

where k is the Boltzmann constant, T is the cell temperature, $a(E)$ is the absorptivity ($a(E) = 1 - \exp[-2 \cdot \alpha(E) \cdot d]$) as previously defined elsewhere [3,40], d is the film thickness ($d = 500$ nm), $\alpha(E)$ is the energy-dependent absorption coefficient, $\phi_{sun}(E)$ is the AM1.5 spectral photon flux, and $\phi_{bb}(E)$ is the blackbody spectral photon flux all as a function of energy, E .

Importantly, and as discussed in depth previously [38,39], photon recycling is implicit in the Shockley-Queisser detailed balance calculation, where the total photon flux emitted from the front surface of the device is used to determine the external radiative saturation current: $J_0^{rad,ext}$ (Eq. 3). Here, only the emitted photons in the escape cone contribute to $J_0^{rad,ext}$, regardless of the number of photon recycling events before escape (see Supplemental Material for discussion of the escape cone [31]) [37,41].

Next, we determine the benefits of photon recycling by considering the radiative saturation current when photon recycling is not included in the calculation [37,42]. The internal radiative saturation current ($J_0^{rad,int}$) is similar to the external radiative saturation current but is enhanced by the photon mode density within the photoactive dielectric medium characterized by the index of refraction, $n_r(E)$, absorption coefficient, and integrated over the sphere of emission [38]. Equation 4 describes a microscopic view of recombination *within* the active region where all photons immediately escape into the surrounding environment [37,41]:

$$(4) \quad J_0^{rad,int}(V) = qe^{\frac{qV}{kT}} \int_0^\infty 4\pi n_r^2(E) \alpha(E) \phi_{bb}(E) dE$$

We use $J_0^{rad,int}$ to calculate the intrinsic carrier density (van Rosebroeck-Shockley relationship, Eq. 5) from standard reported second-order internal radiative recombination rate constants (k_2^{int}) for triple-cation films, $k_2^{int} = 2 \times 10^{-10} \text{ cm}^{-3} \text{ s}^{-1}$ [17,29,43]. The radiative recombination rate constant is an intrinsic material property for a given perovskite film composition, and is not varied in this analysis. We find the external radiative recombination rate constant (k_2^{ext}) and intrinsic carrier density to be $k_2^{ext} = 1 \times 10^{-11} \text{ cm}^{-3} \text{ s}^{-1}$ and $n_i = 2.3 \times 10^5 \text{ cm}^{-3}$ respectively (see Supplemental Material for the determination of k_2^{ext} and n_i [31]), which agree with experimental reports considering photon recycling effects [17,24,43–45].

$$(5) \quad k_2^{int} n_i^2 = \int_0^\infty 4\pi n_r^2(E) \alpha(E) \Phi_{bb}(E) dE$$

In order to make our calculations relevant for real-world perovskite devices exhibiting band-tailing likely due to disorder [46,47], we experimentally determined the energy-dependent absorption coefficient and refractive index using photothermal deflection spectroscopy and ellipsometry (see Supplemental Material Fig. S8 and S19 [31]). Figure 1 shows the theoretical current-voltage (J-V) curves for a triple-cation perovskite solar cell (see Supplemental Material for equivalent curves with $\text{CH}_3\text{NH}_3\text{PbI}_3$ [31]) in the radiative limit with and without photon recycling, calculated using the external and internal radiative saturation currents, respectively. We note that the calculated maximum efficiency with photon recycling of 30.2% corroborates previously reported theoretical limits for a similar bandgap $\text{CH}_3\text{NH}_3\text{PbI}_3$ perovskite solar cell [29], where the theoretical J_{sc} (25.77 mA cm^{-2}) is only slightly higher than what has been achieved experimentally (25.40 mA cm^{-2} [48]). These results emphasize the need to optimize V_{oc} and fill-factor (FF) through reducing non-radiative recombination and harnessing photon recycling.

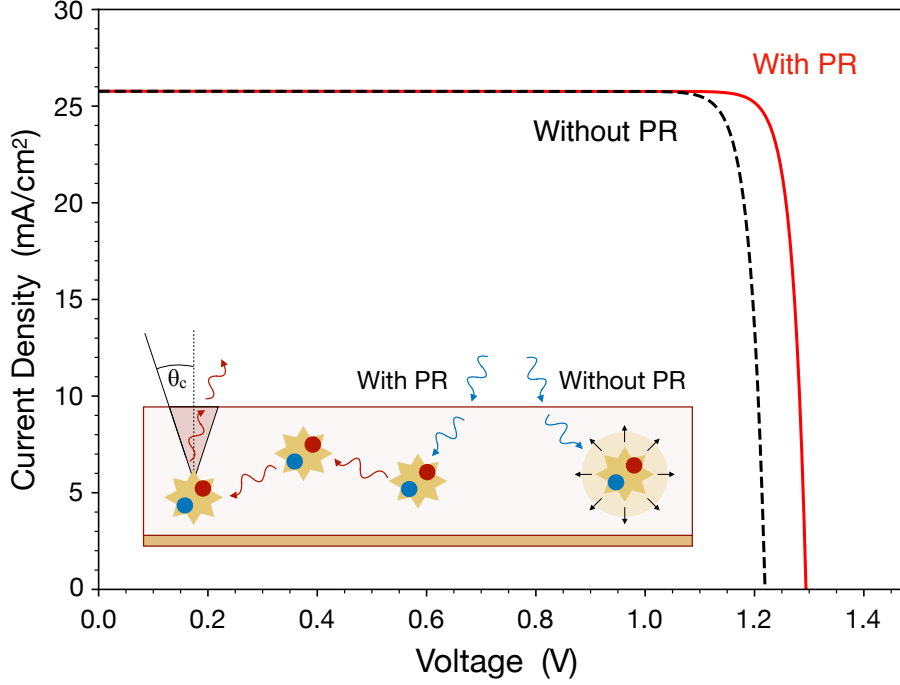


Figure 1. Detailed-balance simulation of J - V curves for an ideal $Cs_{0.05}(MA_{0.17}FA_{0.83})_{0.95}Pb(I_{0.83}Br_{0.17})_3$ perovskite photovoltaic device in the radiative limit (no non-radiative recombination) with (red trace) and without (black dashed trace) photon recycling (PR).

	J_{sc} [mA/cm ²]	V_{oc} [V]	FF	J_{MPP} [mA/cm ²]	V_{MPP} [V]	PCE [%]
No PR	25.77	1.22	0.899	25.19	1.12	28.2
With PR	25.77	1.29	0.906	25.23	1.20	30.2

Table 1. J - V characteristics and power conversion efficiency (PCE) extracted from the simulated J - V curve in the radiative limit with and without photon recycling (PR). Photon recycling leads primarily to enhancements in the maximum power point (MPP) operating voltage (V_{MPP}).

Table 1 shows that photon recycling improves PV device performance at both open-circuit and MPP conditions. The V_{oc} increase of $\Delta V_{oc}^{PR} = 70$ mV calculated in this work is consistent with the 70 mV value predicted by Kirchartz *et al.* for a planar device architecture with Beer-Lambert absorption [29]. Extending beyond previous studies, our full J - V simulation also shows that photon recycling improves the MPP voltage V_{MPP} ($\Delta V_{MPP}^{PR} = 80$ mV) and the FF, producing

an absolute increase in PCE of 2.0%. We note that the short-circuit current density remains unchanged because, with or without photon recycling, J_{SC} only depends on the absorptivity of the material and the solar irradiance.

One highlight of this analysis is that the maximum V_{OC} achievable without photon recycling is only 1.22 V for both the triple-cation and $\text{CH}_3\text{NH}_3\text{PbI}_3$ films (see Supplemental Material Fig. S22 [31]) — a voltage deficit of 0.38 V for each formulation. Our results suggest that perovskite PVs (with bandgap of 1.6 eV) exhibiting $V_{OC} > 1.22$ V and $V_{MPP} > 1.12$ V benefit from photon recycling [32,36]. In this regard, Liu *et al.* recently reported a record-setting $V_{OC} = 1.26$ V in $\text{CH}_3\text{NH}_3\text{PbI}_3$ devices, of which our calculations suggest 40 meV can be attributed to photon recycling effects.

B. Incorporating Non-Radiative Recombination

Theoretical photovoltaic performance limits are useful for setting efficiency targets, but most absorber layers perform far from the radiative limit due to non-radiative losses. Perovskites are no exception – typical films exhibit PLQEs of <15% at 1-sun equivalent generation, with k_1 ranging from 10^6 s⁻¹ to 10^9 s⁻¹, depending on chemical composition and processing methods [13,16,17]. However, with recently developed passivation techniques, k_1 values have been decreasing and will likely continue to decrease as passivation mechanisms are better understood and implemented [14]. For example, a low non-radiative recombination rate of $k_1 = 1.7 \times 10^5$ s⁻¹ has been reported for tri-*n*-octylphosphine oxide (TOPO)-treated $\text{CH}_3\text{NH}_3\text{PbI}_3$ films [18].

To adapt our model to non-idealized scenarios, we modify the saturation current density (Eq. 3 and Eq. 4) to account for non-radiative Shockley-Read-Hall (SRH) and Auger recombination, as previously reported by Pazos-Outón *et al.* (Eq. 6) [29]:

$$(6) \quad J_0 = J_0^{rad} + J_0^{nonrad} = J_0^{rad} + J_{SRH} + J_A$$

where J_0^{rad} is the radiative recombination rate (external or internal) and J_0^{nonrad} is the sum of the non-radiative, first-order SRH (J_{SRH}) and non-radiative, third-order Auger (J_A) recombination

currents. The SRH and Auger recombination rates are described for a carrier density (n) in quasi-thermal equilibrium using the law of mass action (Eq. 7):

$$(7) \quad n(V) = n_i e^{\frac{qV}{2kT}}$$

$$(8) \quad J_{SRH}(V) = qk_1 n(V)d$$

$$(9) \quad J_A(V) = qk_3 n^3(V)d$$

where n_i is the intrinsic carrier density and k_1 and k_3 are the first-order SRH and third-order Auger recombination rate constants, respectively.

Figure 2 shows the impact of different non-radiative recombination values on device performance with and without photon recycling. For these calculations, we used the radiative rate of $k_2^{\text{int}} = 2 \times 10^{-10} \text{ cm}^{-3} \text{ s}^{-1}$ and the Auger rate of $k_3 = 1 \times 10^{-28} \text{ cm}^6 \text{ s}^{-1}$, which are intrinsic material properties that do not vary significantly with film quality (see Supplemental Material for discussion on model sensitivity to k_2^{int} and k_3 [31]) [17,43]. Figure 2a shows the simulated J-V curves with $k_1 = 1 \times 10^4 \text{ s}^{-1}$, which closely resembles those reported in Figure 1 ($k_1 = 0$), suggesting that radiative recombination outcompetes non-radiative recombination and the benefits of photon recycling are therefore observed at this low k_1 . Figure 2b shows that, as k_1 increases to $2 \times 10^5 \text{ s}^{-1}$, the effect of photon recycling is greatly reduced and eventually becomes negligible when non-radiative rates approach $3 \times 10^6 \text{ s}^{-1}$ (Fig. 2c).

Figure 2d shows both the V_{OC} and V_{MPP} with and without photon recycling for varying k_1 values. For k_1 exceeding a threshold value of $2 \times 10^6 \text{ s}^{-1}$ (i.e. $\tau_1 < 500 \text{ ns}$), we observe no increase in V_{OC} and V_{MPP} with photon recycling. For k_1 between $7 \times 10^5 \text{ s}^{-1}$ and $2 \times 10^6 \text{ s}^{-1}$ (i.e. $\tau_1 = 500 \text{ ns}$ to 1430 ns), photon recycling can improve V_{OC} but the fill-factor decreases and, therefore, PCE enhancements are negligible (see Supplemental Material Fig. S9 [31]). With the full J-V simulation we can see that V_{MPP} is unaffected at these values. Only when k_1 is reduced below $7 \times 10^5 \text{ s}^{-1}$ ($\tau_1 > 1430 \text{ ns}$) does photon recycling improve the MPP and efficiency (Figs. S9 and S10). For example, at $k_1 = 2 \times 10^5 \text{ s}^{-1}$ (Fig. 2b), photon recycling increases V_{OC} by 50 mV but V_{MPP}

by only 20 mV (Table 2). We note that for $k_1 = 3 \times 10^6 \text{ s}^{-1}$, the PCE is comparable to current record-performing devices [49].

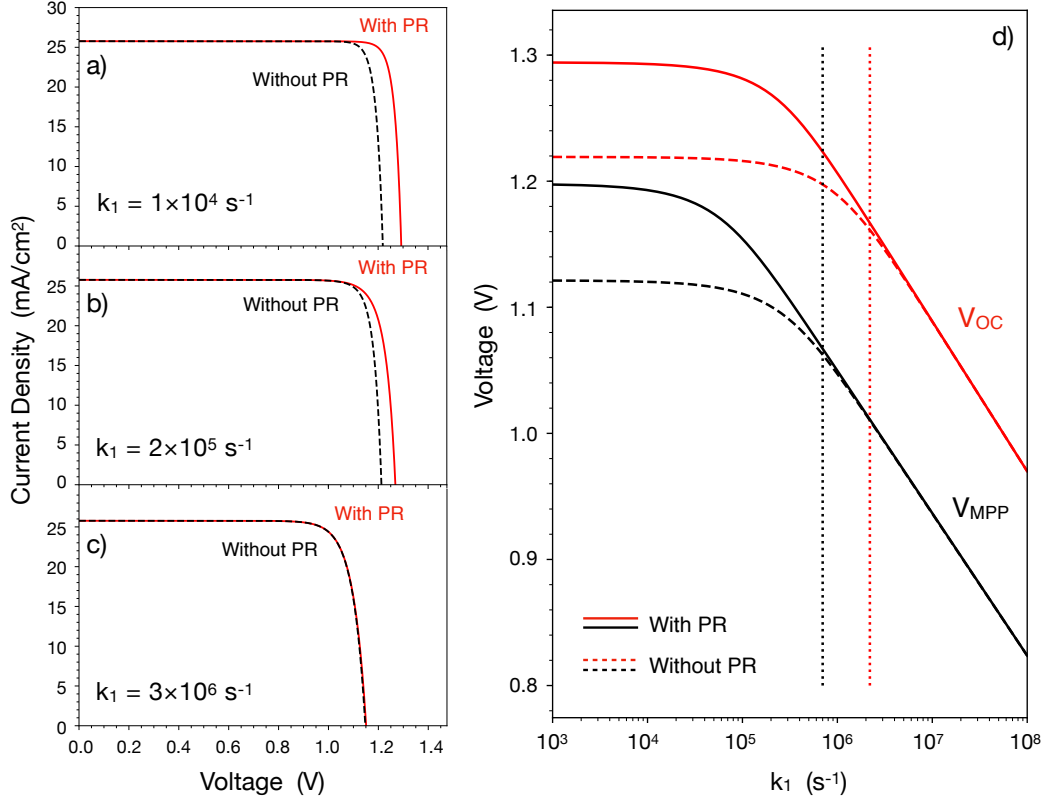


Figure 2. Simulated J - V curves (triple-cation, 1.6 eV bandgap) with and without photon recycling (PR) for k_1 values of (a) $1 \times 10^4 \text{ s}^{-1}$, (b) $2 \times 10^5 \text{ s}^{-1}$, and (c) $3 \times 10^6 \text{ s}^{-1}$ ($k_2^{int} = 2 \times 10^{-10} \text{ cm}^3 \text{ s}^{-1}$ and $k_3 = 1 \times 10^{-28} \text{ cm}^6 \text{ s}^{-1}$). (d) V_{OC} (red lines) and V_{MPP} (black lines) as a function of k_1 , revealing differences in the onset of performance improvements due to PR. Dotted vertical red and black lines indicate k_1 thresholds ($2 \times 10^6 \text{ s}^{-1}$ and $7 \times 10^5 \text{ s}^{-1}$, respectively) below which PR improves performance at open-circuit and the maximum power point (MPP), respectively.

		J_{SC} [mA/cm ²]	V_{OC} [V]	FF	J_{MPP} [mA/cm ²]	V_{MPP} [V]	PCE [%]
$k_1 = 1 \times 10^4 \text{ s}^{-1}$	No PR	25.77	1.22	0.897	25.13	1.12	28.2
	With PR	25.77	1.29	0.900	25.17	1.19	30.0
$k_1 = 2 \times 10^5 \text{ s}^{-1}$	No PR	25.77	1.21	0.876	24.86	1.10	27.4
	With PR	25.77	1.27	0.850	24.67	1.13	27.8
$k_1 = 3 \times 10^6 \text{ s}^{-1}$	No PR	25.77	1.15	0.824	24.50	1.00	24.4
	With PR	25.77	1.15	0.822	24.50	1.00	24.4

Table 2. Device parameters extracted from the simulated J-V curves for $k_1 = 1 \times 10^4$, 2×10^5 , and $3 \times 10^6 \text{ s}^{-1}$ ($k_2^{int} = 2 \times 10^{-10} \text{ cm}^3 \text{ s}^{-1}$ and $k_3 = 1 \times 10^{-28} \text{ cm}^6 \text{ s}^{-1}$) with and without photon recycling (PR).

C. Competition Between Radiative and Non-Radiative Recombination Currents

To better understand the recombination processes governing PV device behavior with and without photon recycling, we break down the J-V curve from Figure 2b ($k_1 = 2 \times 10^5 \text{ s}^{-1}$) into its individual recombination components. The absolute magnitude is calculated using Equations 3-4 and 8-9, and the fraction of each recombination mechanism is its magnitude divided by the total recombination current (i.e. $J_{SRH,rad,A} / J_{tot}$).

Figures 3a and b show $J_0^{rad,int}$ and $J_0^{rad,ext}$ as a function of voltage, along with J_{SRH} and J_A , which are the SRH and Auger non-radiative pathways, respectively. J_{SRH} and J_A have the same functional form with or without photon recycling, as neither depend on the radiative saturation current (Eqs. 8-9). Photon recycling requires the reabsorption of emitted photons; if the recombination process is non-radiative (i.e. SRH, Auger), no photons are generated for the reabsorption process. We observe that photon recycling shifts radiative recombination to higher onset voltages and therefore reduces the magnitude of the radiative saturation current at MPP, leading to increases in V_{OC} and V_{MPP} with photon recycling (Table 2, $k_1 = 2 \times 10^5 \text{ s}^{-1}$). Figures 3c and d give further insight into these results, where the fractions of each recombination current are compared as a function of voltage. With photon recycling, SRH recombination becomes the limiting pathway (solid blue and red traces). To harness photon recycling in devices, it is essential to reduce non-radiative recombination pathways through improved processing or passivation

techniques. For example, alkali metal salt additives and interfacial passivation layers have yielded low voltage-deficit devices (e.g. <0.35 V) which we predict currently benefit from, but do not fully harness, photon recycling [36,50].

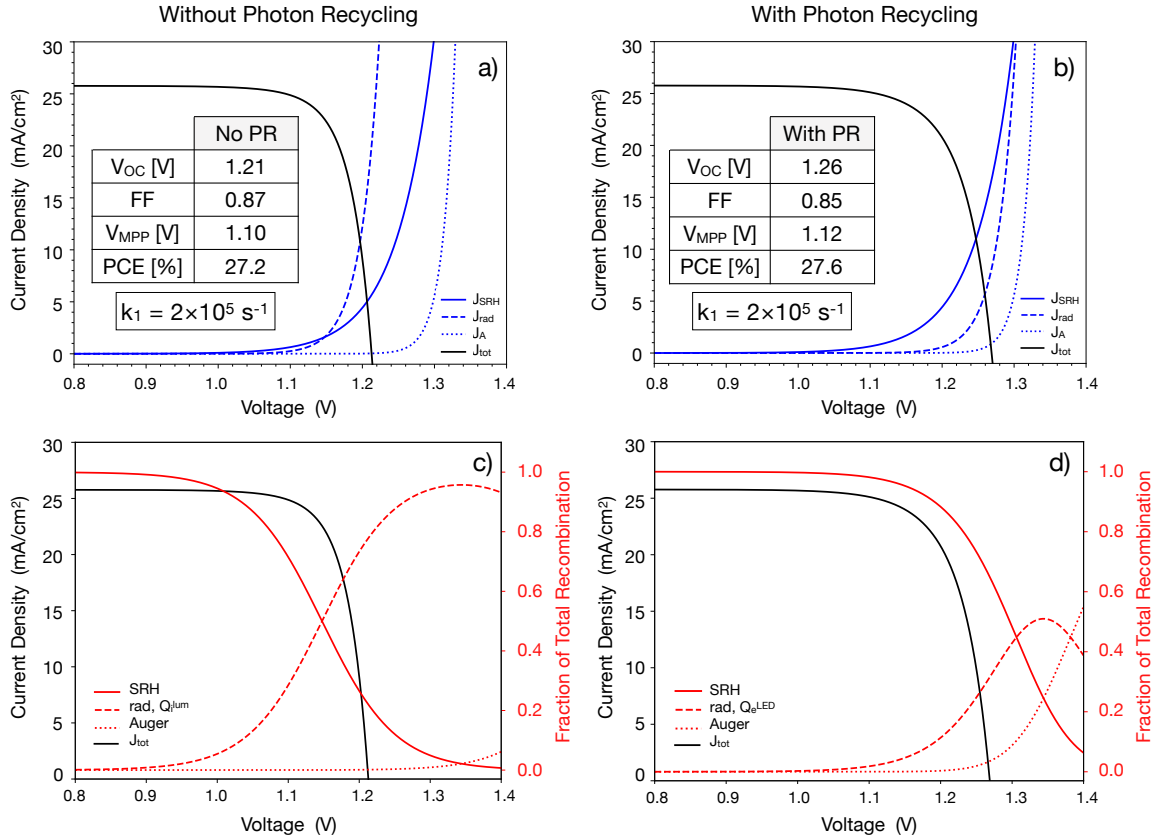


Figure 3. Simulated J - V curves (black traces) for $k_1 = 2 \times 10^5 \text{ s}^{-1}$, $k_2^{int} = 2 \times 10^{-10} \text{ cm}^3 \text{ s}^{-1}$, and $k_3 = 1 \times 10^{-28} \text{ cm}^6 \text{ s}^{-1}$ (a, c) without and (b, d) with photon recycling (PR) are shown with the magnitude of Shockley-Read-Hall (SRH), radiative, and Auger recombination currents as a function of voltage (blue traces). (c, d) The fractions of total recombination current due to SRH, radiative, and Auger recombination are shown at each voltage (red traces) (c) without and (d) with PR. The fraction of radiative recombination as a function of voltage with and without PR is equivalent to Q_e^{LED} and Q_i^{lum} , respectively.

We note that the radiative recombination fraction without photon recycling in Figure 3c is equal to the internal luminescence quantum efficiency (Q_i^{lum}), which has similarly been defined elsewhere [38]:

$$(10) \quad Q_i^{\text{lum}}(V) = \frac{J_0^{\text{rad,int}}(V)}{J_{\text{SRH}}(V) + J_0^{\text{rad,int}}(V) + J_A(V)}$$

The radiative recombination fraction with photon recycling in Figure 3d yields the external light-emitting diode (LED) electroluminescence efficiency (Q_e^{LED}), which is connected to the mean probability of photon escape from the film (P_{esc}) through a geometric series [38]:

$$(11) \quad Q_e^{\text{LED}}(V) = \frac{P_{\text{esc}} Q_i^{\text{lum}}(V)}{1 - Q_i^{\text{lum}}(V)(1 - P_{\text{esc}})}$$

Here, the escape probability (P_{esc}) can be defined as the ratio of the external to the internal radiative saturation current [38]:

$$(12) \quad P_{\text{esc}} = \frac{J_0^{\text{rad,ext}}}{J_0^{\text{rad,int}}}$$

III. External Electroluminescence Efficiency Enhancements

Q_e^{LED} is a function of the injection current, and thus it is necessary to denote both the injection current and corresponding voltage at which the current is achieved for a given Q_e^{LED} . Due to the reciprocity relations that link optical output to electrical input, Q_e^{LED} values are often measured at an injection current equivalent to the photocurrent [51,52]. Unless otherwise stated, we report Q_e^{LED} values calculated with an injection current equivalent to J_{SC} – i.e. applied voltage equal to V_{OC} , $Q_e^{\text{LED}}(V_{\text{OC}})$. Considering Equation 11, Figure 3d shows that a device with $k_1 = 2 \times 10^5 \text{ s}^{-1}$ (i.e. $\tau_1 = 5 \text{ }\mu\text{s}$) should demonstrate a $Q_e^{\text{LED}}(V_{\text{OC}})$ of 31.5%. Importantly, the external emission efficiency of a solar cell is a metric that has been shown to directly correlate with power conversion efficiency and, therefore, serves as a useful optimization parameter [53,54]. Equations 9 and 10 provide two apparent routes: decreasing J_{SRH} and J_A and/or increasing P_{esc} to increase $Q_e^{\text{LED}}(V_{\text{OC}})$. To evaluate which method best capitalizes on the benefits of photon recycling, we examine the dependence of $Q_e^{\text{LED}}(V_{\text{OC}})$ and P_{esc} on V_{OC} and V_{MPP} .

A. Modification of Non-Radiative Recombination

First, we consider how $Q_e^{\text{LED}}(V_{\text{OC}})$ and photovoltage are affected by decreasing J_{SRH} (i.e. varying k_1 in Equation 8), for a fixed escape probability ($P_{\text{esc}} = 4.7\%$). Figure 4 shows $Q_e^{\text{LED}}(V_{\text{OC}})$ increases with decreasing k_1 , resulting in voltage enhancements at open-circuit and MPP. We report a photon recycling threshold of $Q_e^{\text{LED}}(V_{\text{OC}}) > \sim 0.3\%$ and significant performance improvements for $Q_e^{\text{LED}}(V_{\text{OC}}) = 10\%$, yielding $\Delta V_{\text{OC}}^{\text{PR}} = 36$ mV and $\Delta V_{\text{MPP}}^{\text{PR}} = 9$ mV (Fig. 4). Recently, Liu *et al.* reported a $Q_e^{\text{LED}}(V_{\text{OC}})$ of $7.5 \pm 2.5\%$ for $\text{CH}_3\text{NH}_3\text{PbI}_3$ devices achieving a V_{OC} of 1.26 V. This experimental V_{OC} is higher than the maximum achievable theoretical V_{OC} in the radiative limit without photon recycling, indicating performance enhancements due to photon recycling [36].

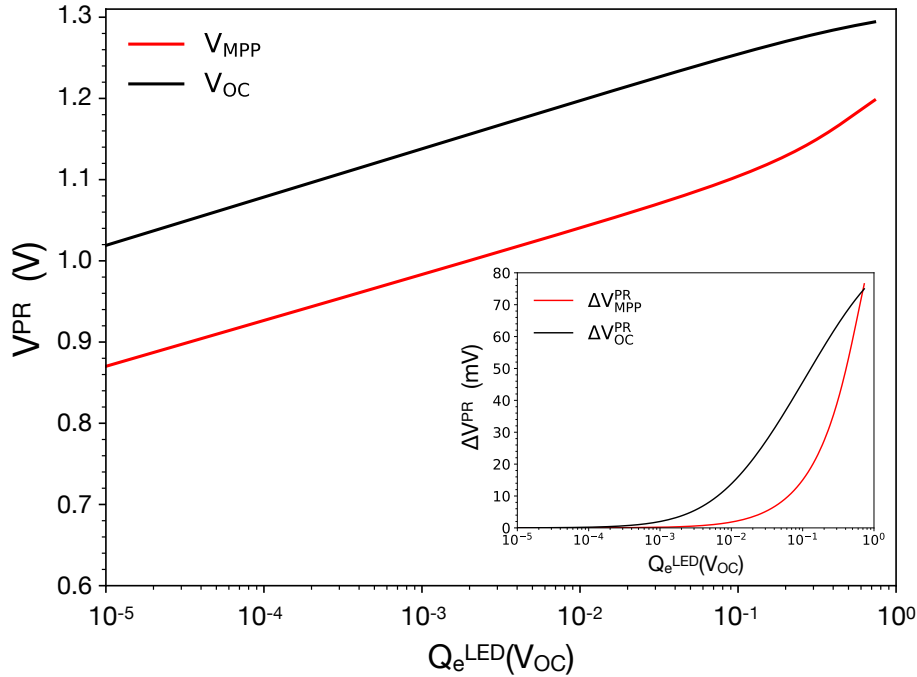


Figure 4. The voltage with photon recycling (V^{PR}) for $P_{\text{esc}} = 4.7\%$ at the maximum power point (MPP) and open-circuit is shown as a function of $Q_e^{\text{LED}}(V_{\text{OC}})$, which, as non-radiative recombination decreases, approaches unity. Inset: ΔV^{PR} for $P_{\text{esc}} = 4.7\%$ at MPP and open-circuit as a function of $Q_e^{\text{LED}}(V_{\text{OC}})$.

B. Modification of Probability of Photon Escape

Second, we consider how $Q_e^{\text{LED}}(V_{OC})$ and photovoltage (see below) are affected by increasing P_{esc} and decreasing k_1 . We note that the photovoltage is proportional to the steady-state carrier density and is, therefore, an intuitive metric to compare across the multiple varying parameters. We calculate the carrier density using the law of mass action (Eq. 7) as a function of k_1 and P_{esc} .

Figure 5a shows that, at $P_{esc} = 4.7\%$ and low k_1 values, photon recycling increases the steady-state carrier density by a factor of four, from 8.5×10^{14} to $3.7 \times 10^{15} \text{ cm}^{-3}$ at MPP. This high carrier density results from additional generation associated with the reabsorption of trapped photons — up to 18-suns equivalent at open circuit and >1.4 equivalent suns at MPP (see Supplemental Material Figs. S12 and S13 for triple-cation and Fig. S27 for $\text{CH}_3\text{NH}_3\text{PbI}_3$ [31]). Figure 5 shows that photon recycling allows $Q_e^{\text{LED}}(V_{OC})$ to exceed the escape probability (see Supplemental Material Figs. S14 and S15 [31]), a direct result from the multiple re-absorption events that re-randomize the photon propagation angle. While the emission efficiency can increase beyond P_{esc} as non-radiative recombination decreases, $Q_e^{\text{LED}}(V_{OC})$ cannot reach 100% due to the higher fraction of Auger recombination at increased steady-state carrier densities, as shown in Figure 3c-d. A similar limiting effect for the efficiency droop at high applied voltages in GaN LEDs has been attributed to Auger recombination processes [55,56].

Next, we consider scenarios in which P_{esc} is changed without significantly impacting the material absorptivity function (see Supplemental Material for model assumptions [31]). Figures 5b and 5c show the carrier density and $Q_e^{\text{LED}}(V_{OC})$ for $P_{esc} = 9.4\%$ and 14.1% . Here, the steady-state carrier density steadily decreases, while $Q_e^{\text{LED}}(V_{OC})$ approaches 90% with photon recycling due to a smaller contribution from Auger recombination at lower carrier densities. These results appear to counteract one another, as both a high steady-state carrier density and high $Q_e^{\text{LED}}(V_{OC})$ are desired.

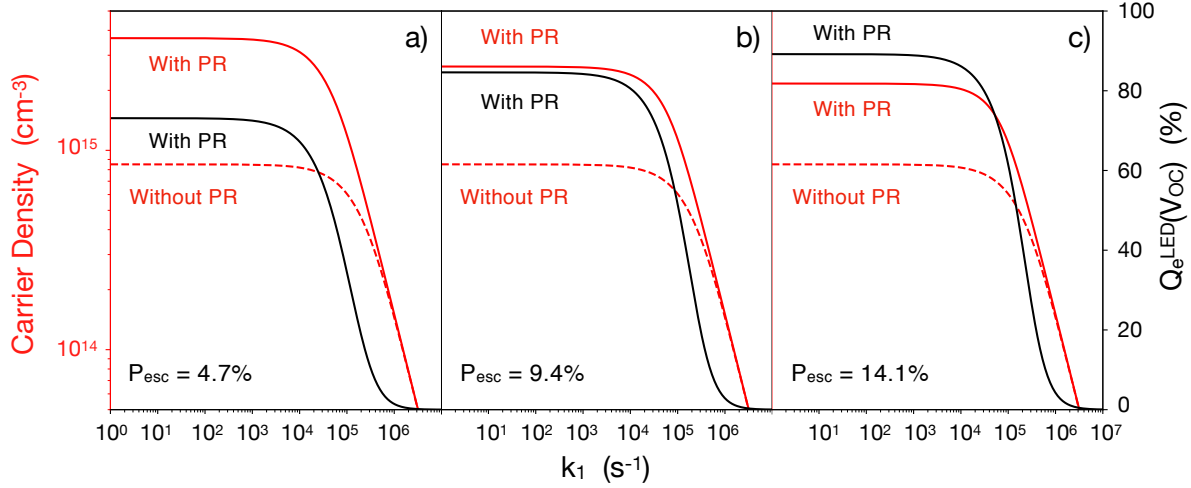


Figure 5. The effect of photon recycling (PR) on the maximum power point (MPP) steady-state carrier density and $Q_e^{\text{LED}}(V_{OC})$ as a function of k_1 for a) $P_{esc} = 4.7\%$, b) 9.4% , and c) 14.1% .

This observation raises the question as to whether solely increasing the escape probability can enhance device performance and, in particular, open-circuit voltage [15,16]. The traditional definition of the maximum achievable open-circuit voltage (V_{OC}^{max}) is expressed as a function of the external LED electroluminescence efficiency, as described in Equation 13 [38,51,57].

$$(13) \quad V_{OC}^{\text{max}} = V_{OC}^{\text{rad}} + \frac{kT}{q} \ln[Q_e^{\text{LED}}(V_{OC})]$$

Here, it appears that increasing $Q_e^{\text{LED}}(V_{OC})$ through enhancing the escape probability should allow V_{OC}^{max} to approach V_{OC}^{rad} – however, the implicit dependence of the radiative component (V_{OC}^{rad}) on P_{esc} is often overlooked. This dependence becomes clear if we equate $J_0^{\text{rad,ext}}$ with the product of $J_0^{\text{rad,int}}$ and P_{esc} (Eq. 14), where it can be seen that this term decreases as the escape probability increases [58].

$$(14) \quad V_{OC}^{\text{rad}} = \frac{kT}{q} \ln\left[\frac{J_{SC}}{J_0^{\text{rad,ext}}}\right] = \frac{kT}{q} \ln\left[\frac{J_{SC}}{P_{esc} J_0^{\text{rad,int}}}\right]$$

IV. Effect of Non-Radiative Recombination and Probability of Escape on V_{OC}

To better understand the competition between V_{OC}^{rad} and $Q_e^{LED}(V_{OC})$ on V_{OC}^{max} , Figures 6a and b show the magnitude of these terms as a function of P_{esc} and k_1 . As P_{esc} increases for a given k_1 , V_{OC}^{rad} decreases due to the enhanced light outcoupling, which increases the external radiative saturation current. Opposing this negative impact on V_{OC}^{max} from V_{OC}^{rad} , V_{OC}^{nonrad} also decreases with increasing P_{esc} , resulting in a smaller subtractive component from V_{OC}^{max} , as shown in Figure 6b. As P_{esc} changes, the radiative and non-radiative terms vary in opposing directions.

Ultimately, V_{OC}^{max} is dominated by the radiative dependence on P_{esc} , so V_{OC}^{max} decreases monotonically with increasing P_{esc} at a constant k_1 value (Fig. 6c) [16]. Thus, it is evident that simply increasing the outcoupling efficiency reduces output voltages due to the reduction in steady-state carrier density (c.f. Fig. 5). We highlight that we only analyze the voltage in this simulation, and note that overall device performance may not track the changes in voltage if, for example, J_{SC} also changes.

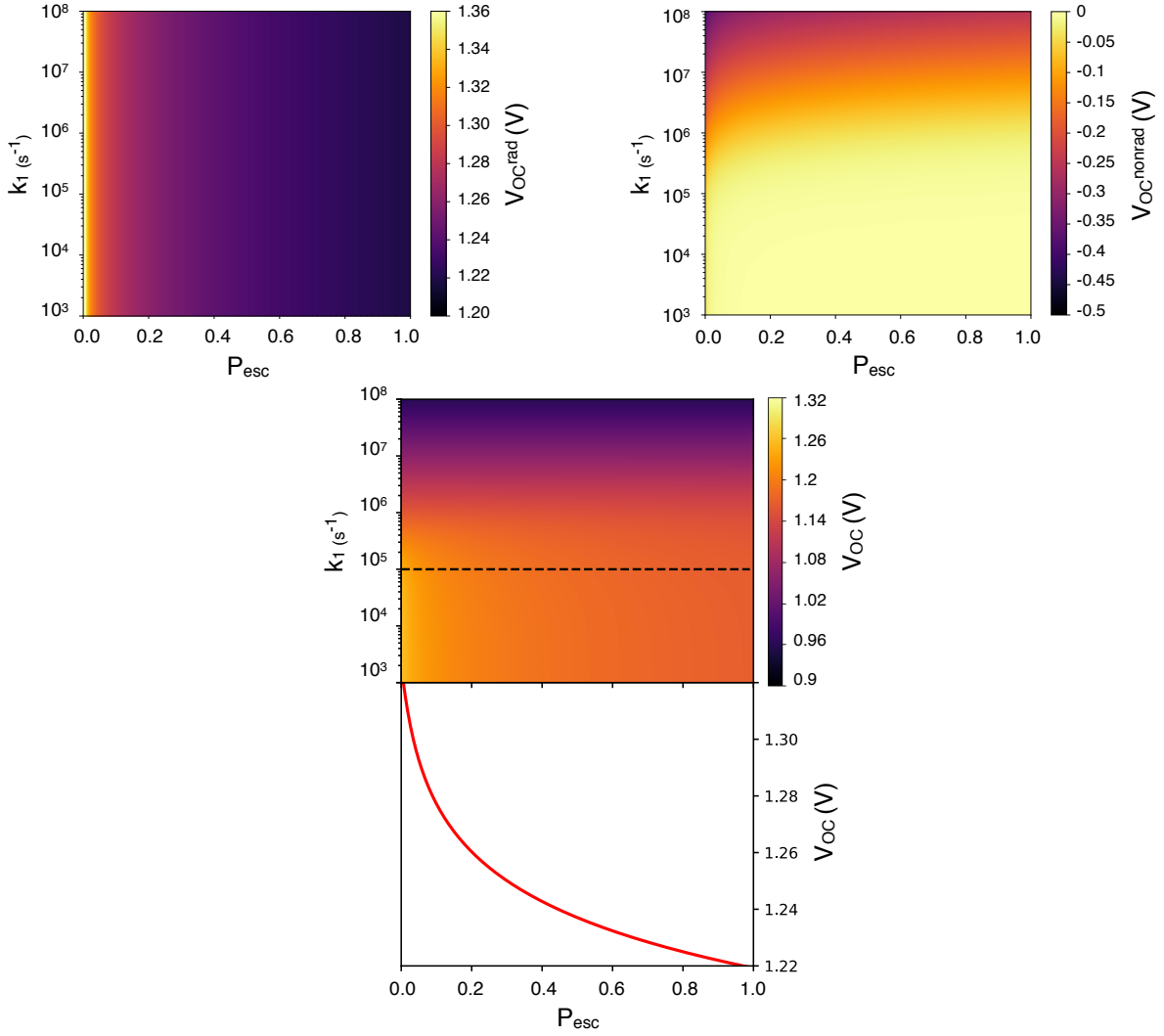


Figure 6. a) The V_{OC} with photon recycling (PR) in the radiative limit (V_{OC}^{rad}) is shown along with b) the non-radiative subtractive effect on V_{OC}^{max} (V_{OC}^{nonrad}). Combined, $V_{OC}^{rad} + V_{OC}^{nonrad}$ yield c) the total V_{OC}^{max} as a function of k_1 and P_{esc} , with a dashed line at $k_1 = 1 \times 10^5 s^{-1}$ showing that increasing P_{esc} for a fixed Q_i^{lum} decreases V_{OC} .

V. Conclusion

In summary, we present a rigorous method for evaluating the extent of and benefits from photon recycling in emerging perovskite absorbers by exploring device performance limits using experimentally determined optical constants and absorption for triple-cation films. This analysis investigates the effect of photon recycling on both V_{OC} and operationally-relevant maximum power point (MPP) parameters, both in the radiative limit and with non-radiative recombination. Our simulations provide a framework for evaluating the improvements attributable to photon recycling in standard current-voltage measurements. This analysis reveals that perovskite devices demonstrating voltage deficits of <0.38 V [32,36] already benefit from photon recycling. This would mean that high-quality devices fabricated today may be further improved by reducing non-radiative recombination and/or modifying the escape probability to harness the benefits of photon recycling.

With recycling, photons waveguided within the film can be re-absorbed and re-emitted in the escape cone, allowing $Q_e^{LED}(V_{OC})$ to approach the intrinsic limit while maintaining a high steady-state carrier density. If $Q_e^{LED}(V_{OC})$ is enhanced only by increasing P_{esc} , the steady-state carrier density will decrease, resulting in a lower V_{OC} . For triple-cation films, enhancements in V_{OC} and V_{MPP} are observed for $k_1 < 2 \times 10^6$ s⁻¹ ($\tau_1 > 500$ ns) and $k_1 < 7 \times 10^5$ s⁻¹ ($\tau_1 > 1430$ ns), respectively, while, for $k_1 < 1 \times 10^4$ s⁻¹ ($\tau_1 > 100$ μ s), further performance improvements become negligible. Our analysis, therefore, identifies a target non-radiative recombination rate for perovskite films of $k_1 < 1 \times 10^4$ s⁻¹. Below this threshold, the steady-state carrier density plateaus at $4 \times$ the density without photon recycling. In theory, a perovskite film reaching this lower bound of $k_1 = 1 \times 10^4$ s⁻¹ ($P_{esc} = 4.7\%$) can achieve a 74 mV increase in V_{OC} , 73 mV improvement in V_{MPP} , 0.3% absolute increase in fill factor, and 1.79% increase in PCE — due solely to photon recycling.

We note that the model used to simulate J-V curves in this study represents an ideal case and sets an upper limit for the target non-radiative recombination rate constants. For example, perovskite material quality will likely need to be even better than these targets, as charge transport layers in devices introduce new pathways for interfacial recombination. Passivation methods and surface modifiers that reduce the number of defects at the interfaces and lead to favorable band alignment will be critical in minimizing non-radiative loss to fully harness photon

recycling [18,24,25]. Toward the development of new perovskite formulations and device architectures, this analysis provides clear material quality targets and device performance limits for evaluating photon recycling in next-generation perovskite solar cells.

Acknowledgments

This work is supported by the TATA-MIT GridEdge Solar Research program. This material is based upon work supported by the National Science Foundation Graduate Research Fellowship under Grant No. (1122374). We would also like to acknowledge support from NSF/CBET-BSF under Grant No. 1605406 (EP/L000202). We thank Dak Benjia Dou for his guidance in the preparation of the triple cation perovskite thin films; Nina Hong, from J.A. Woollam Co., Inc., for her technical support analyzing the ellipsometry data; and Luis Pazos-Outón and Thomas Mahony for valuable discussions.

References

- [1] E. Yablonovitch, Lead halides join the top optoelectronic league, *Science* **351**, 1401 (2016).
- [2] O. D. Miller and E. Yablonovitch, Photon extraction: the key physics for approaching solar cell efficiency limits, *Proc. SPIE* **8808**, 880807 (2013).
- [3] O. D. Miller, E. Yablonovitch, and S. R. Kurtz, Strong internal and external luminescence as solar cells approach the Shockley-Queisser limit, *IEEE J. Photovoltaics* **2**, 303 (2012).
- [4] M. A. Steiner, J. F. Geisz, I. García, D. J. Friedman, A. Duda, and S. R. Kurtz, Optical enhancement of the open-circuit voltage in high quality GaAs solar cells, *J. Appl. Phys.* **113**, 123109 (2013).
- [5] R. K. Ahrenkiel, D. J. Dunlavy, B. Keyes, S. M. Vernon, T. M. Dixon, S. P. Tobin, K. L. Miller, and R. E. Hayes, Ultralong minority-carrier lifetime epitaxial GaAs by photon recycling, *Appl. Phys. Lett.* **55**, 1088 (1989).
- [6] A. W. Walker, O. Höhn, D. N. Micha, B. Bläsi, A. W. Bett, and F. Dimroth, Impact of Photon Recycling on GaAs Solar Cell Designs, *IEEE J. Photovoltaics* **5**, 1636 (2015).
- [7] A. Braun, E. A. Katz, D. Feuermann, B. M. Kayes, and J. M. Gordon, Photovoltaic performance enhancement by external recycling of photon emission, *Energy Environ. Sci.* **6**, 1499 (2013).
- [8] F. Staub, H. Hempel, J.-C. Hebig, J. Mock, U. W. Paetzold, U. Rau, T. Unold, and T. Kirchartz, Beyond Bulk Lifetimes: Insights into Lead Halide Perovskite Films from Time-Resolved Photoluminescence, *Phys. Rev. Appl.* **6**, 044017 (2016).
- [9] F. Staub, T. Kirchartz, K. Bittkau, and U. Rau, Manipulating the Net Radiative Recombination Rate in Lead Halide Perovskite Films by Modification of Light Outcoupling, *J. Phys. Chem. Lett.* **8**, 5084 (2017).
- [10] R. K. Ahrenkiel, B. M. Keyes, G. B. Lush, M. R. Melloch, M. S. Lundstrom, and H. F. MacMillan, Minority-carrier lifetime and photon recycling in *n*-GaAs, *J. Vac. Sci. Technol. A* **10**, 990 (1992).
- [11] J. L. Balenzategui and A. Martí, Detailed modelling of photon recycling: Application to GaAs solar cells, *Sol. Energy Mater. Sol. Cells* **90**, 1068 (2006).
- [12] P. Renaud, F. Raymond, B. Bensaïd, and C. Vérié, Influence of photon recycling on lifetime and diffusion coefficient in GaAs, *J. Appl. Phys.* **71**, 1907 (1992).
- [13] L. M. Pazos-Outon, M. Szumilo, R. Lamboll, J. M. Richter, M. Crespo-Quesada, M. Abdi-Jalebi, H. J. Beeson, M. Vruini, M. Alsari, H. J. Snaith, B. Ehrler, R. H. Friend, and F. Deschler, Photon recycling in lead iodide perovskite solar cells, *Science* **351**, 1430 (2016).
- [14] Y. Fang, H. Wei, Q. Dong, and J. Huang, Quantification of re-absorption and re-emission processes to determine photon recycling efficiency in perovskite single crystals, *Nat. Commun.* **8**,

- 14417 (2017).
- [15] W. Tress, Perovskite Solar Cells on the Way to Their Radiative Efficiency Limit – Insights Into a Success Story of High Open-Circuit Voltage and Low Recombination, *Adv. Energy Mater.* **7**, 1602358 (2017).
- [16] J. M. Richter, M. Abdi-Jalebi, A. Sadhanala, M. Tabachnyk, J. P. H. Rivett, L. M. Pazos-Outón, K. C. Gödel, M. Price, F. Deschler, and R. H. Friend, Enhancing photoluminescence yields in lead halide perovskites by photon recycling and light out-coupling, *Nat. Commun.* **7**, 13941 (2016).
- [17] M. B. Johnston and L. M. Herz, Hybrid Perovskites for Photovoltaics: Charge-Carrier Recombination, Diffusion, and Radiative Efficiencies, *Acc. Chem. Res.* **49**, 146 (2016).
- [18] D. W. Dequilettes, S. Koch, S. Burke, R. K. Paranj, A. J. Shropshire, M. E. Ziffer, and D. S. Ginger, Photoluminescence Lifetimes Exceeding 8 μ s and Quantum Yields Exceeding 30% in Hybrid Perovskite Thin Films by Ligand Passivation, *ACS Energy Lett.* **1**, 438 (2016).
- [19] Q. Dong, Y. Fang, Y. Shao, P. Mulligan, J. Qiu, L. Cao, and J. Huang, Electron-hole diffusion lengths > 175 μ m in solution-grown $\text{CH}_3\text{NH}_3\text{PbI}_3$ single crystals, *Science* **347**, 967 (2015).
- [20] Y. Fang, Q. Dong, Y. Shao, Y. Yuan, and J. Huang, Highly narrowband perovskite single-crystal photodetectors enabled by surface-charge recombination, *Nat. Photonics* **9**, 679 (2015).
- [21] Y. Yamada, T. Yamada, and Y. Kanemitsu, Free Carrier Radiative Recombination and Photon Recycling in Lead Halide Perovskite Solar Cell Materials, *Bull. Chem. Soc. Jpn.* **90**, 1129 (2017).
- [22] T. Yamada, Y. Yamada, Y. Nakaike, A. Wakamiya, and Y. Kanemitsu, Photon Emission and Reabsorption Processes in $\text{CH}_3\text{NH}_3\text{PbBr}_3$ Single Crystals Revealed by Time-Resolved Two-Photon-Excitation Photoluminescence Microscopy, *Phys. Rev. Appl.* **7**, 014001 (2017).
- [23] Y. Kanemitsu, Luminescence spectroscopy of lead-halide perovskites: materials properties and application as photovoltaic devices, *J. Mater. Chem. C* **5**, 3427 (2017).
- [24] R. Brenes, D. Guo, A. Osherov, N. K. Noel, C. Eames, E. M. Hutter, S. K. Pathak, F. Niroui, R. H. Friend, M. S. Islam, H. J. Snaith, V. Bulović, T. J. Savenije, and S. D. Stranks, Metal Halide Perovskite Polycrystalline Films Exhibiting Properties of Single Crystals, *Joule* **1**, 155 (2017).
- [25] M. Abdi-Jalebi, Z. Andaji-Garmaroudi, S. Cacovich, C. Stavrakas, B. Philippe, J. M. Richter, M. Alsari, E. P. Booker, E. M. Hutter, A. J. Pearson, S. Lilliu, T. J. Savenije, H. Rensmo, G. Divitini, C. Ducati, R. H. Friend, and S. D. Stranks, Maximizing and stabilizing luminescence from halide perovskites with potassium passivation, *Nature* **555**, 497 (2018).
- [26] I. Schnitzer, E. Yablonovitch, C. Caneau, and T. J. Gmitter, Ultrahigh spontaneous emission quantum efficiency, 99.7% internally and 72% externally, from AlGaAs/GaAs/AlGaAs double heterostructures, *Appl. Phys. Lett.* **62**, 131 (1993).
- [27] M. Saliba, T. Matsui, J.-Y. Seo, K. Domanski, J.-P. Correa-Baena, M. K. Nazeeruddin, S. M.

- Zakeeruddin, W. Tress, A. Abate, A. Hagfeldt, and M. Grätzel, Cesium-containing triple cation perovskite solar cells: Improved stability, reproducibility and high efficiency, *Energy Environ. Sci.* **9**, 1989 (2016).
- [28] J. A. Christians, P. Schulz, J. S. Tinkham, T. H. Schloemer, S. P. Harvey, B. J. Tremolet de Villers, A. Sellinger, J. J. Berry, and J. M. Luther, Tailored interfaces of unencapsulated perovskite solar cells for >1,000 hour operational stability, *Nat. Energy* **3**, 68 (2018).
- [29] L. M. Pazos-Outón, T. P. Xiao, and E. Yablonovitch, Fundamental Efficiency Limit of Lead Iodide Perovskite Solar Cells, *J. Phys. Chem. Lett.* **9**, 1703 (2018).
- [30] S. M. Durbin and J. L. Gray, Numerical modeling of photon recycling in solar cells, *IEEE Trans. Electron Devices* **41**, 239 (1994).
- [31] See Supplemental Material at [URL will be inserted by publisher] for full experimental methods, model assumptions, absorption spectra and extension of the analysis for $\text{CH}_3\text{NH}_3\text{PbI}_3$ films, (n.d.).
- [32] S. Gholipour and M. Saliba, From Exceptional Properties to Stability Challenges of Perovskite Solar Cells, *Small* **14**, 1802385 (2018).
- [33] M. Saliba, T. Matsui, K. Domanski, J.-Y. Seo, A. Ummadisingu, S. M. Zakeeruddin, J.-P. Correa-Baena, W. R. Tress, A. Abate, A. Hagfeldt, and M. Gratzel, Incorporation of rubidium cations into perovskite solar cells improves photovoltaic performance, *Science* **354**, 206 (2016).
- [34] M. Saliba, J. P. Correa-Baena, C. M. Wolff, M. Stolterfoht, N. Phung, S. Albrecht, D. Neher, and A. Abate, How to Make over 20% Efficient Perovskite Solar Cells in Regular (n-i-p) and Inverted (p-i-n) Architectures, *Chem. Mater.* **30**, 4193 (2018).
- [35] W. Tress, M. Yavari, K. Domanski, P. Yadav, B. Niesen, J. P. Correa Baena, A. Hagfeldt, and M. Graetzel, Interpretation and evolution of open-circuit voltage, recombination, ideality factor and subgap defect states during reversible light-soaking and irreversible degradation of perovskite solar cells, *Energy Environ. Sci.* **11**, 151 (2018).
- [36] Z. Liu, L. Krückemeier, B. Krogmeier, B. Klingebiel, J. A. Márquez, S. Levchenko, S. Öz, S. Mathur, U. Rau, T. Unold, and T. Kirchartz, Open-Circuit Voltages Exceeding 1.26 V in Planar Methylammonium Lead Iodide Perovskite Solar Cells, *ACS Energy Lett.* **4**, 110 (2019).
- [37] T. Kirchartz, F. Staub, and U. Rau, Impact of Photon Recycling on the Open-Circuit Voltage of Metal Halide Perovskite Solar Cells, *ACS Energy Lett.* **1**, 731 (2016).
- [38] U. Rau, U. W. Paetzold, and T. Kirchartz, Thermodynamics of light management in photovoltaic devices, *Phys. Rev. B* **90**, 035211 (2014).
- [39] A. Martí, J. L. Balenzategui, and R. F. Reyna, Photon recycling and Shockley's diode equation, *J. Appl. Phys.* **82**, 4067 (1997).
- [40] J. K. Katahara and H. W. Hillhouse, Quasi-Fermi level splitting and sub-bandgap absorptivity

- from semiconductor photoluminescence, *J. Appl. Phys.* **116**, 173504 (2014).
- [41] J. Bisquert, *The Physics of Solar Cells*, Taylor & Francis Group (CRC Press, Boca Raton, FL, 2018).
- [42] W. van Roosbroeck and W. Shockley, Photon-Radiative Recombination of Electrons and Holes in Germanium, *Phys. Rev.* **94**, 1558 (1954).
- [43] A. Kumar, A. Priyadarshi, S. Shukla, M. Manjappa, L. J. Haur, S. G. Mhaisalkar, and R. Singh, Ultrafast THz photophysics of solvent engineered triple-cation halide perovskites, *J. Appl. Phys.* **124**, 215106 (2018).
- [44] A. Mahboubi Soufiani, Z. Yang, T. Young, A. Miyata, A. Surrente, A. Pascoe, K. Galkowski, M. Abdi-Jalebi, R. Brenes, J. Urban, N. Zhang, V. Bulović, O. Portugall, Y.-B. Cheng, R. J. Nicholas, A. Ho-Baillie, M. A. Green, P. Plochocka, and S. D. Stranks, Impact of microstructure on the electron–hole interaction in lead halide perovskites, *Energy Environ. Sci.* **10**, 1358 (2017).
- [45] T. W. Crothers, R. L. Milot, J. B. Patel, E. S. Parrott, J. Schlipf, P. Müller-Buschbaum, M. B. Johnston, and L. M. Herz, Photon Reabsorption Masks Intrinsic Bimolecular Charge-Carrier Recombination in $\text{CH}_3\text{NH}_3\text{PbI}_3$ Perovskite, *Nano Lett.* **17**, 5782 (2017).
- [46] A. D. Wright, R. L. Milot, G. E. Eperon, H. J. Snaith, M. B. Johnston, and L. M. Herz, Band-Tail Recombination in Hybrid Lead Iodide Perovskite, *Adv. Funct. Mater.* **27**, 1700860 (2017).
- [47] J. Mattheis, U. Rau, and J. H. Werner, Light absorption and emission in semiconductors with band gap fluctuations—A study on $\text{Cu}(\text{In,Ga})\text{Se}_2$ thin films, *J. Appl. Phys.* **101**, 113519 (2007).
- [48] M. A. Green, Y. Hishikawa, E. D. Dunlop, D. H. Levi, J. Hohl-Ebinger, M. Yoshita, and A. W. Y. Ho-Baillie, Solar cell efficiency tables (Version 53), *Prog. Photovoltaics Res. Appl.* **27**, 3 (2019).
- [49] National Renewable Energy Laboratory, Perovskite efficiency chart, NREL (2018).
- [50] S. Yang, J. Dai, Z. Yu, Y. Shao, Y. Zhou, X. Xiao, X. C. Zeng, and J. Huang, Tailoring Passivation Molecular Structures for Extremely Small Open-Circuit Voltage Loss in Perovskite Solar Cells, *J. Am. Chem. Soc.* **141**, 5781 (2019).
- [51] U. Rau, Reciprocity relation between photovoltaic quantum efficiency and electroluminescent emission of solar cells, *Phys. Rev. B* **76**, 085303 (2007).
- [52] W. Tress, N. Marinova, O. Inganäs, M. K. Nazeeruddin, S. M. Zakeeruddin, and M. Graetzel, Predicting the Open-Circuit Voltage of $\text{CH}_3\text{NH}_3\text{PbI}_3$ Perovskite Solar Cells Using Electroluminescence and Photovoltaic Quantum Efficiency Spectra: the Role of Radiative and Non-Radiative Recombination, *Adv. Energy Mater.* **5**, 1400812 (2015).
- [53] M. A. Green and S. P. Bremner, Energy conversion approaches and materials for high-efficiency photovoltaics, *Nat. Mater.* **16**, 23 (2017).
- [54] M. A. Green, Radiative efficiency of state-of-the-art photovoltaic cells, *Prog. Photovoltaics Res.*

- Appl. **20**, 472 (2012).
- [55] J. Iveland, L. Martinelli, J. Peretti, J. S. Speck, and C. Weisbuch, Direct Measurement of Auger Electrons Emitted from a Semiconductor Light-Emitting Diode under Electrical Injection: Identification of the Dominant Mechanism for Efficiency Droop, *Phys. Rev. Lett.* **110**, 177406 (2013).
- [56] E. Kioupakis, P. Rinke, K. T. Delaney, and C. G. Van de Walle, Indirect Auger recombination as a cause of efficiency droop in nitride light-emitting diodes, *Appl. Phys. Lett.* **98**, 161107 (2011).
- [57] R. T. Ross, Some Thermodynamics of Photochemical Systems, *J. Chem. Phys.* **46**, 4590 (1967).
- [58] M. G. Abebe, A. Abass, G. Gomard, L. Zschiedrich, U. Lemmer, B. S. Richards, C. Rockstuhl, and U. W. Paetzold, Rigorous Treatment of Photon Recycling in Thermodynamics of Photovoltaics: The Case of Perovskite Thin-Film Solar Cells, *Phys. Rev. B* **98**, 075141 (2018).